NOAA Technical Memorandum OAR ARL-246

A STATISTICAL INVESTIGATION OF ATMOSPHERIC DISPERSION AT THE IDAHO NATIONAL ENGINEERING AND ENVIRONMENTAL LABORATORY (INEEL)

R.M. Eckman

Field Research Division
Idaho Falls, Idaho

Air Resources Laboratory
Silver Spring, Maryland
February 2003

noaa NATIONAL OCEANIC AND ATMOSPHERIC ADMINISTRATION / Oceanic and Atmospheric Research Laboratories

NOAA Technical Memorandum OAR ARL-246

A STATISTICAL INVESTIGATION OF ATMOSPHERIC DISPERSION AT THE IDAHO NATIONAL ENGINEERING AND ENVIRONMENTAL LABORATORY (INEEL)

Richard M. Eckman

Field Research Division
Idaho Falls, Idaho

Air Resources Laboratory
Silver Spring, Maryland
February 2003

UNITED STATES DEPARTMENT OF COMMERCE

Donald L. Evans
Secretary

NATIONAL OCEANIC AND ATMOSPHERIC ADMINISTRATION

VADM Conrad C. Lautenbacher, Jr.
Under Secretary for Oceans and Atmosphere/Administrator

Oceanic and Atmospheric Research Laboratories

David L. Evans
Director

NOTICE

Mention of a commercial company or product does not constitute an endorsement by NOAA. Use for publicity or advertising purposes, of information from this publication concerning proprietary products or the tests of such products, is not authorized.

Contents

List of Figures

A Statistical Investigation of Atmospheric Dispersion at the Idaho National Engineering and Environmental Laboratory (INEEL)

Richard M. Eckman

ABSTRACT. A study of worst-case dispersion events is presented for the Idaho National Engineering and Environmental Laboratory (INEEL) in Southeastern Idaho. It is based on nine years of meteorological data from an extensive tower network around INEEL. These data were used as input to a puff dispersion model, which provided estimates of the total integrated concentration over a domain surrounding INEEL. With nine years of data, it was possible to generate probability density functions (pdfs) for the model's total integrated concentration ψ_m. Worst-case dispersion events were then defined as the 95th percentile values of ψ_m from these pdfs.

Two different pdfs are considered for ψ_m. The first has no restrictions on time, date, or meteorological conditions, and therefore has many null values representing cases when the model plume totally misses the chosen receptor location. The second pdf excludes these nulls since it is conditional on the plume reaching the receptor location at some point during the model run. This pdf generally gives larger values of ψ_m for the worst-case events. Overall, the worst-case events are clearly affected by the northeast-southwest channeling of the wind within the Snake River Plain where INEEL is located. However, more localized flows due to nearby mountains are also important.

The report demonstrates that there are many possible quantitative definitions of worst-case dispersion. Past studies at INEEL have used different definitions, but the end users of these studies may not have been aware of this. It is unclear whether this may have led to incorrect planning decisions. Choosing the best definition of worst-case dispersion for risk assessment is ultimately a policy decision rather than a strictly scientific issue.

Another issue addressed in the report is that all the INEEL worst-case dispersion studies (including this study) are based solely on model estimates ψ_m of the integrated concentration. No consideration has been given to how ψ_m relates to the *actual* integrated concentration ψ at the receptor location. The relation between ψ_m and ψ is shown to be associated with another pdf representing the model uncertainty. Conceptually, the uncertainty can be addressed using probability theory. However, a proper assessment of the uncertainty was beyond the scope of this study. Nonetheless, users of this study and previous INEEL dispersion studies should be aware that the effects of model uncertainty on the worst-case estimates were not addressed.

1. Introduction

The Idaho National Engineering and Environmental Laboratory (INEEL) is one of several national laboratories operated by the U.S. Department of Energy. It is located in a semidesert area of Southeast Idaho known as the Eastern Snake River Plain (Fig. 1). This plain has a southwest–northeast axis with higher elevations toward the northeast. Although the topography within the INEEL boundaries is relatively flat, several mountain ranges with peaks exceeding 3000 m AGL are just west and north of the site. The site's vegetation is dominated by sagebrush and grasses (Anderson et al. 1996).

Several different facilities are located within the INEEL. Many of them store nuclear materials, and some have operational nuclear reactors. Many also use chemical materials that present a health risk if they were accidentally released into the atmosphere. The INEEL must therefore conduct planning studies of the possible consequences related to accidental releases of chemical and nuclear materials into the atmosphere. For radiological dose assessment, the INEEL has used a straight-line Gaussian plume model called the Radiological Safety Analysis Computer Program [RSAC, see Wenzel and Schrader (2001) for a description of the latest version].

For consequence assessment, one is often attempting to come up with a worst-case scenario. The worst-case scenarios for the INEEL facilities appear to have been initially based on RSAC runs using what has been called the "95% weather conditions" (Einerson 1994). These conditions correspond to Pasquill-Gifford stability class F with a wind speed

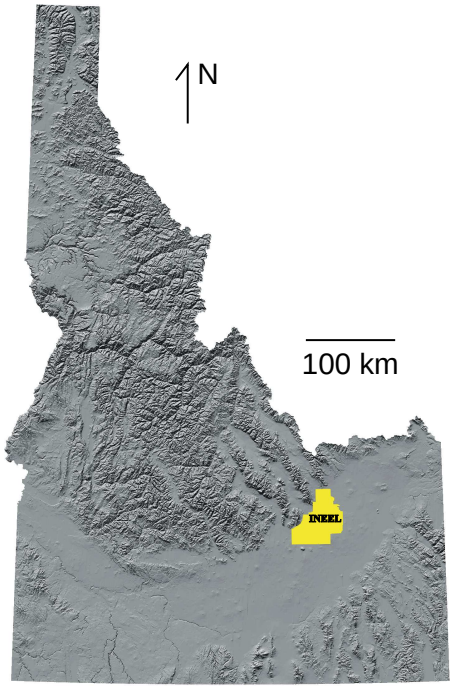

Figure 1: Map of Idaho with INEEL as shaded area.

of 1 m s^{-1} for nearly all the INEEL facilities. This is in agreement with the rule of thumb that most dispersion meteorologists use in describing worst-case scenarios for a surface release. The radiological dose assessments for the INEEL facilities were originally based on RSAC runs using this combination of wind speed and stability (Bonney 1997).

RSAC is a straight-line Gaussian plume model, so it assumes that the pollutant at some downwind distance x has experienced the same transport wind and turbulence levels since it exited the source. Near the source, this is a reasonable assumption, but it becomes increasingly unrealistic further downwind. At 30 km downwind, for example, the pollutant would have to experience unchanging 95% weather conditions over about 8 hours. This problem led some to question the RSAC results at longer ranges downwind.

In the mid 1990s, the Field Research Division (FRD) of the NOAA Air Resources Laboratory was asked to perform some independent worst-case dispersion estimates using real wind data from a tower network operated by FRD. A preliminary study was based on one year of data from the network, and a later study used three years of data. The results of the later study are given in Sagendorf (1996). This study used a version of the MDIFF puff model (Sagendorf et al. 2001). Since a puff model can account for temporal and spatial variations in the wind and turbulence, there is no restriction to straight-line transport as in RSAC. Based on the three-year data set, Sagendorf (1996) made estimates of the 95th percentile concentration at each grid point in the model domain. In most cases the MDIFF 95th percentile concentrations were less than the corresponding values from RSAC based on the 95% weather conditions. Bonney (1997) used the MDIFF statistics to estimate 95th percentile radiological doses for the INEEL facilities.

INEEL has recently asked FRD to conduct an updated version of the Sagendorf (1996) study using a longer-term data set. About nine years of data are currently available from the FRD tower network, compared with the three years available to Sagendorf. INEEL is interested in knowing whether the longer data record has much effect on the concentration statistics.

This report describes the updated statistical study of dispersion at INEEL. The discussion begins in Section 2 with a consideration of the *definition* and *interpretation* of worst-case dispersion statistics. These are important issues, because quantifying a worst-case dispersion event is more complicated than it first appears. A lack of awareness of these complexities may have resulted in misinterpretations of the Sagendorf (1996) statistics. It is not clear whether these misinterpretations may have led to incorrect planning decisions at INEEL. Later sections in the report describe the puff model used in the INEEL dispersion study, its configuration, and finally the results of the modeling.

2. How Do We Define the Worst-Case Dispersion?

Qualitatively, the concept of the "worst-case" dispersion event is relatively simple. For a given source location and source strength, it is generally taken to represent a combination

of meteorological conditions that gives the highest ground-level concentrations χ downwind of the source. However, when one attempts to quantify this concept, things become more complicated. In looking over the INEEL consequence assessments that have been performed based on the Sagendorf (1996) study, it appears that the worst-case statistics were sometimes misinterpreted. This section considers the concept of worst-case dispersion events in more detail, with the hope of avoiding future misinterpretations.

2.1. Definitions Based on Probability Theory

We start with the qualitative definition of worst-case given in the preceding paragraph. The highest ground-level concentrations are expected to be directly along the plume centerline for surface releases and beneath the centerline for elevated releases. This definition therefore implies that we focus on estimating how χ varies with downwind distance x_c along (or under) the plume centerline. Suppose we let the symbol I represent our prior knowledge about a particular pollutant source and the local meteorology near this source. (I may also include assumptions related to a specific modeling approach.) In a probabilistic context, we can then define $p(\chi \,|\, x_c, I)$ as the probability density function (pdf) for χ, conditional upon downwind distance x_c along the plume centerline and our other assumptions embodied in I. The common concept of worst-case dispersion is clearly related in some way to the upper tail of $p(\chi \,|\, x_c, I)$.

One problem that immediately arises with this pdf is that the concentration χ is somewhat loosely defined. In real plumes the concentration at x_c will vary in time, but no such time dependence is indicated in the pdf. One solution to this problem is to interpret χ as some kind of peak concentration observed at x_c. Alternatively, χ can represent some kind of average or expectation concentration. This latter interpretation is particularly relevant for straight-line Gaussian plume models such as RSAC, because these models are designed to provide the average concentration resulting from a steady-state release.

The Einerson (1994) computations of worst-case dispersion at INEEL are essentially a computation of $p(\chi \,|\, x_c, I)$ based on observed INEEL meteorology and the RSAC model. As noted above, χ in this context represents an average concentration. In the Gaussian plume framework, the mean wind speed U and a parameter s representing atmospheric stability are two of the main meteorological variables affecting the dispersion. The sum and product rules for probabilities then give the expansion

$$p(\chi \,|\, x_c, I) = \int dU \int p(U, s \,|\, I)\, p(\chi \,|\, x_c, I, U, s)\, ds \,, \tag{1}$$

where the integral limits are determined by the allowable range of speeds and stabilities. The pdf $p(\chi \,|\, x_c, I, U, s)$ provides the distribution of χ conditional upon specific values of U and s. The joint pdf $p(U, s \,|\, I)$ is associated with the probability of specific wind speed and stability combinations given prior knowledge of the local meteorology at the source. Einerson (1994) solved a discrete version of Eq. (1) by relating $p(\chi \,|\, x_c, I, U, s)$ to the output of RSAC and $p(U, s \,|\, I)$ to wind and stability frequency distributions derived from INEEL tower observations. The RSAC combination of F stability class and $U = 1 \,\mathrm{m\,s^{-1}}$

came closest to the 95th percentile of $p(\chi \,|\, x_c, I)$ for most INEEL facilities, so this combination became known as the "95% weather conditions".

If we take the 95th percentile of $p(\chi \,|\, x_c, I)$ to represent worst-case dispersion, it is important to remember that this pdf only considers what is happening on the ground along (or under) the plume centerline. It has only one spatial dimension x_c, and therefore has no dependence on the wind direction and says nothing about what is happening off the centerline axis. This point appears to have been missed in Bonney (1997), where it is stated that the Einerson (1994) computations produce circular concentration isopleths about the source. The wind-direction dependence has been marginalized in $p(\chi \,|\, x_c, I)$, so this pdf says nothing about the shape of concentration isopleths around the release point.

If we want to consider the effects of wind direction tendencies in a worst-case analysis, we clearly do not want to use $p(\chi \,|\, x_c, I)$. In a more general context, a receptor can be located at some distance r and direction D from the pollutant source. The direction D need not have any relation to prevailing wind directions. Assuming we are still mainly interested in ground-level concentrations χ at the position (r, D), we can consider the pdf $p(\chi \,|\, r, D, I)$, where I again represents our prior knowledge of the source and local meteorology. It is clear that the 95th percentile of $p(\chi \,|\, r, D, I)$ will usually be substantially less than $p(\chi \,|\, x_c, I)$ at $x_c = r$, simply because the plume will not invariably "hit" the receptor at (r, D). In fact, just a basic knowledge of wind-direction variability would lead one to believe that the probability of a plume hit is less then 50% for most receptor locations that are an appreciable distance from the source. The pdf $p(\chi \,|\, r, D, I)$ therefore includes a large number of null concentrations for the times when the plume misses the receptor.

The Sagendorf (1996) study appears to represent a computation of $p(\chi \,|\, r, D, I)$ using the MDIFF puff model and three years of meteorological data. (As discussed in the next subsection, there is some confusion about whether the Sagendorf study is based on the concentration χ or a different variable.) The 95th percentile contours in the Sagendorf report are from this pdf. These contours are not symmetric about the source, since the prevailing winds in the Snake River Plain make some directions D more likely to be hit by the plume than others.

Sagendorf (1996) also presents contour plots of median (50th percentile) concentrations. He discovered during the analysis, however, that the median of $p(\chi \,|\, r, D, I)$ was zero except for a small area near each INEEL source. This confirms our expectation that most receptor locations have less than a 50% chance of being hit by the plume. The median plots given in the report were therefore based on another pdf that was derived from $p(\chi \,|\, r, D, I)$ by removing the null concentrations.

Suppose we use the symbol H to denote the case when the plume "hits" the receptor at (r, D). A hit can be defined as a case when the plume passes close enough to (r, D) that χ exceeds some lower detection threshold. The pdf $p(\chi \,|\, r, D, I)$ can then be subdivided into mutually exclusive cases where H is true and cases where it is false (denoted by $\overline{H}$). The sum and product rules for probabilities then allow the pdf to be expanded as

$$p(\chi \,|\, r, D, I) = P(H \,|\, r, D, I)\, p(\chi \,|\, r, D, I, H) + P(\overline{H} \,|\, r, D, I)\, p(\chi \,|\, r, D, I, \overline{H})\,, \qquad (2)$$

where $P(H \mid r, D, I)$ is the probability (not pdf) of a "hit" and $P(\overline{H} \mid r, D, I)$ is the probability of a "miss". Both of these quantities are probabilities rather than pdfs, since H is either true or false. They must also obey the relation $P(\overline{H} \mid r, D, I) = 1 - P(H \mid r, D, I)$.

The pdf $p(\chi \mid r, D, I, H)$ in Eq. (2) represents the distribution of χ when H is given as true. The other pdf $p(\chi \mid r, D, I, \overline{H})$ represents the case when H is false. Since $\overline{H}$ implies the concentration must be zero (or indistinguishable from zero), this latter pdf must be a delta function at zero concentration:

$$p(\chi \mid r, D, I) = P(H \mid r, D, I)\, p(\chi \mid r, D, I, H) + P(\overline{H} \mid r, D, I)\, \delta(\chi)\,. \tag{3}$$

From this equation it is clear that $p(\chi \mid r, D, I)$ will often be bimodal, with one mode at $\chi = 0$ for plume misses and a second mode at a nonzero χ for plume hits. Also, the median of $p(\chi \mid r, D, I)$ will be zero if $P(\overline{H} \mid r, D, I) \geq 0.5$.

Equations (2) and (3) allow us to interpret the Sagendorf (1996) results. He provided contours for the 95th percentile of $p(\chi \mid r, D, I)$ and was also planning to provide median values for this distribution. However, he discovered that $P(\overline{H} \mid r, D, I)$ was greater than 0.5 for most (r, D) in the model domain. Plots of these medians were therefore uninteresting. He instead reported the medians for the pdf $p(\chi \mid r, D, I, H)$ representing only the cases where a plume hit occurred. This pdf of course has a nonzero median. The important point is that Sagendorf's 95th percentiles and medians come from different distributions, and thus are not directly intercomparable.

It is also clear that the worst-case statistics generated by Sagendorf (1996) are not directly comparable with the RSAC statistics considered by Einerson (1994) and Bonney (1997). The RSAC statistics are based on the centerline pdf $p(\chi \mid x_c, I)$ considered early in this section. Sagendorf's statistics are based on the direction-dependent pdfs $p(\chi \mid r, D, I)$ and $p(\chi \mid r, D, I, H)$. Which of these statistics is most relevant to INEEL consequence assessments? There is no uniquely correct answer to this question, because the choice of statistics is ultimately a policy decision rather than a purely scientific issue. If policy makers are interested in the general risk of exposure with no restrictions on time of day, date, or meteorology, then statistics based on $p(\chi \mid r, D, I)$ are probably most relevant. If the interest is in the exposure risk at some location (r, D) assuming that the location has been hit by the plume, then $p(\chi \mid r, D, I, H)$ is more appropriate. If the only concern is the exposure along the plume centerline, then $p(\chi \mid x_c, I)$ is appropriate.

In the puff modeling approach used by Sagendorf (1996), the plume centerline is not fixed in time or space, so it is difficult to generate estimates of $p(\chi \mid x_c, I)$. An approximation to this pdf can be obtained by marginalizing D in $p(\chi \mid r, D, I, H)$:

$$p(\chi \mid r, I, H) = \frac{1}{2\pi} \int_0^{2\pi} p(\chi \mid r, D, I, H)\, dD\,. \tag{4}$$

This pdf is still not exactly equal to $p(\chi \mid x_c, I)$, since the plume may hit a location along the radius r without the centerline actually passing over the location.

2.2. Choice of Dependent Variable

In Section 2.1 the worst-case events were associated with the ground-level concentration χ. It was implied in this discussion that the χ values must represent some kind of peak or average value, since in real plumes the concentration varies with time. Within the Gaussian plume approach of RSAC, the interpretation of χ is fairly simple. Each model run produces a single concentration value at a specific location, representing the average concentration from a steady-state source. It therefore makes sense in the Gaussian plume context to base the worst-case events on χ values. Usually, the concentration is normalized by the source release rate q, so the variable used in the risk assessment becomes χ/q. If χ has units of Ci m^{-3} and q units of Ci s^{-1}, then χ/q has units of s m^{-3}.

In Einerson (1994), Bonney (1997), and Sagendorf (1996), the worst-case estimates were reported as χ/q in s m^{-3}. However, a problem arises in the Sagendorf study because puff models like MDIFF allow the concentration to vary with time. Each MDIFF run produces a time series of χ at a location (r, D) rather than a single value. It is therefore unclear how a single χ value is extracted from this time series. This issue was well known to the MDIFF developers, so instead of χ, the output variable in MDIFF is actually the time integrated concentration ψ, sometimes called the exposure:

$$\psi(r, D, t_o, T_s) = \int_{t_o}^{t_o+T_s} \chi(r, D, t)\, dt\,. \tag{5}$$

Here, t_o is the model start time and T_s is the length of the model simulation. Since MDIFF tracks puffs until they exit the model domain or dilute below a threshold, T_s is effectively infinity. Sagendorf (1996) appears to have assumed that a χ/q value could be obtained from MDIFF by normalizing ψ with the product qt_r, with t_r being the assumed duration of the release.

Since q was assumed to be constant over t_r, the product qt_r actually represents the total quantity Q (in, say, Ci) of material released from the source. The variable reported by Sagendorf was therefore in actuality the ratio ψ/Q. This happens to have the same units (*e.g.*, s m^{-3}) as χ/q, but does that mean these ratios are equivalent? In a puff model these quantities are clearly different. For a single MDIFF simulation, a particular location (r, D) will only be exposed to the plume over a limited time T_e. Our definition of exposure is related to the idea of a plume hit discussed above, in that a location is being exposed any time the concentration exceeds a detection threshold. An average exposure concentration can then be defined as

$$\chi_e = \frac{\psi}{T_e}\,, \tag{6}$$

representing the average concentration over the periods (which may not be contiguous) when the receptor was exposed to the plume. We could then use the ratio χ_e/q in our assessment planning.

With q assumed constant over the release period, we have

$$\frac{\chi_e}{q} = \frac{\psi}{Q}\frac{t_r}{T_e}\,. \tag{7}$$

This shows that χ_e/q and ψ/Q are only equivalent when the receptor exposure time T_e equals the duration t_r of the release. In a puff model there is no universal relation between T_e and t_r. For example, most of the model simulations reported in Section 4 are based on $t_r = 1$ h, but T_e can vary anywhere from several minutes to many hours.

An estimation of worst-case events based on ψ/Q will not be the same as one based on χ_e/q. High values of ψ/Q are likely to be associated with longer exposure times T_e. In contrast, high values of χ_e/q may be associated with high concentrations but short exposure times. Since the INEEL consequence assessments are directed at radiological exposure, it would seem that ψ/Q is the more appropriate choice. This ratio is used in the later sections of this report. Some care must be taken in matching a puff model ψ/Q to straight-line plume results, because the standard Gaussian-plume approach does not include either t_r or T_e as part of the original model derivation. These concepts are applied later in the application of the model results to real plumes, and the times are assumed to be equal. Equation (7) then shows that ψ/Q and χ_e/q must be equal in a straight-line plume model. Hence, there is no distinction in a plume model between a worst-case ψ/Q and a worst-case χ_e/q.

2.3. Model Estimation of Worst-Case Dispersion

The discussion in the foregoing subsection led to the conclusion that estimates of worst-case dispersion for INEEL should be based on the ratio ψ/Q, with ψ assumed to be at ground level. For some receptor location at a distance r and direction D from the source, we can define $p(\psi/Q \,|\, r, D, I)$ to represent the pdf for ψ/Q given r, D, and our other knowledge I of the source and local meteorology. This pdf is similar to $p(\chi \,|\, r, D, I)$ in Section 2.1 except for the change in the dependent variable.

A straightforward way to estimate $p(\psi/Q \,|\, r, D, I)$ with a dispersion model is to make repeated model runs using long records of meteorological data. If the meteorological records are sufficiently long, they can be assumed to provide a reasonable representation of the meteorological conditions that can be expected in the future. A large number n of model runs based on these data will provide n estimates of ψ/Q at each point (r, D). The frequency distribution of these estimates can than be interpreted as representing the pdf $p(\psi/Q \,|\, r, D, I)$. Sagendorf (1996) used three years of data from towers at INEEL to estimate this pdf. Approximately nine years of data are now available; model runs from this longer set of records should presumably provide more stable estimates of the pdf.

Using repeated runs of a dispersion model to estimate $p(\psi/Q \,|\, r, D, I)$ appears relatively simple, but it requires a major assumption that is easy to overlook. The density $p(\psi/Q \,|\, r, D, I)$ that is of interest for risk assessment represents inferences about the *actual* integrated concentration at the receptor location. However, a model is only providing *estimated* values ψ_m, which contain some uncertainty. We therefore must in general consider a joint pdf $p(\psi/Q, \psi_m/Q \,|\, r, D, I_m)$ for both the actual ψ and modeled ψ_m integrated concentrations. The prior information I_m in this case includes knowledge of the

specific model that generates ψ_m. This pdf can be expanded by the product rule as

$$p(\psi/Q, \psi_m/Q \,|\, r, D, I_m) = p(\psi_m/Q \,|\, r, D, I_m)\, p(\psi/Q \,|\, \psi_m/Q, r, D, I_m)\,. \tag{8}$$

The first factor on the right side is the pdf for the model estimate ψ_m. This is the distribution that is actually being estimated by making repeated runs of a dispersion model. The second factor represents how the actual values ψ are distributed for a given model estimate. In other words, this factor is related to the model uncertainty.

An integral equation for $p(\psi/Q \,|\, r, D, I_m)$ can be obtained from Eq. (8) by marginalizing ψ_m/Q:

$$\begin{aligned} p(\psi/Q \,|\, r, D, I_m) &= \int p(\psi/Q, \psi_m/Q \,|\, r, D, I_m)\; d(\psi_m/Q) \\ &= \int p(\psi_m/Q \,|\, r, D, I_m)\, p(\psi/Q \,|\, \psi_m/Q, r, D, I_m)\; d(\psi_m/Q)\,. \end{aligned} \tag{9}$$

This equation shows how the pdf we are really interested in—namely $p(\psi/Q \,|\, r, D, I_m)$—is related to the pdf we can obtain from the modeling, $p(\psi_m/Q \,|\, r, D, I_m)$. To solve this equation we must know something about the model uncertainty, as expressed in $p(\psi/Q \,|\, \psi_m/Q, r, D, I_m)$. As a notational shorthand in the following discussion, we will denote $p(\psi/Q \,|\, r, D, I_m)$ by p_f, $p(\psi_m/Q \,|\, r, D, I_m)$ by p_m, and $p(\psi/Q \,|\, \psi_m/Q, r, D, I_m)$ by p_u.

From Eq. (9), we see that the direct use of the model pdf p_m in consequence assessment, as done by Sagendorf (1996)[1], is equavalent to assuming that p_m has the same shape as p_f. This assumption will be valid in Eq. (9) if the uncertainty pdf p_u is narrowly distributed about $\psi/Q = \psi_m/Q$. (More specifically, p_u must be narrowly distributed relative to the variation of p_m with ψ_m/Q). Generally, one would not expect the model uncertainty to be so narrowly distributed. The final pdf p_f will therefore most likely be broader than the model distribution p_m to reflect this uncertainty.

In concept, the model uncertainty p_u can be estimated using something like a maximum entropy approach (Jaynes 1957; Bretthorst 1996) combined with prior information on the dispersion model's performance. For example, field data might indicate that the model has a systematic bias or tends to have a certain amount of scatter relative to observations. Such information could be used together with a maximum entropy approach to estimate the uncertainty. Unfortunately, this approach is beyond the limited scope and budget of the study reported here. Instead, we fall back on the same approach as Sagendorf and assume p_m is a reasonable substitute for p_f. The consequence of this assumption is that the statistics reported in this report come from a model pdf that is likely narrower than the pdf p_f of ultimate interest.

From the discussion in Section 2.1, there is an expectation that the model pdf $p_m = p(\psi_m/Q \,|\, r, D, I_m)$ will include many null values resulting from plume misses. We can subdivide this pdf in a manner similar to Eq. (3)

$$p(\psi_m/Q \,|\, r, D, I_m) = P(H \,|\, r, D, I_m) p(\psi_m/Q \,|\, r, D, I_m, H) + P(\overline{H} \,|\, r, D, I_m)\delta(\psi_m/Q)\,, \tag{10}$$

[1]Einerson (1994) made a similar assumption in deriving the 95% weather conditions.

with $p(\psi_m/Q \,|\, r, D, I_m, H)$ representing the ψ_m distribution given that a plume hit has occurred, and $P(H \,|\, r, D, I_m)$ representing the probability of a model plume hit. Both of these are easily estimated from the model runs in the same manner as $p(\psi_m/Q \,|\, r, D, I_m)$.

The statistics given later in this report are based on the model distributions of $p(\psi_m/Q \,|\, r, D, I_m)$, $p(\psi_m/Q \,|\, r, D, I_m, H)$, and $P(H \,|\, r, D, I_m)$. The 95th percentiles of $p(\psi_m/Q \,|\, r, D, I_m)$ and $p(\psi_m/Q \,|\, r, D, I_m, H)$ are respectively denoted by A_{95} and C_{95}. Medians C_{50} are also computed for the second pdf so they can be compared with the 95th percentiles. Plots are provided for the probability $P(H \,|\, r, D, I_m)$ to provide some indication of the importance of the second term in Eq. (10). This probability must satisfy the equality $P(H \,|\, r, D, I_m) = 1 - P(\overline{H} \,|\, r, D, I_m)$, so a small value of $P(H \,|\, r, D, I_m)$ implies a large value of $P(\overline{H} \,|\, r, D, I_m)$.

3. Dispersion Modeling for INEEL Facilities

3.1. Puff Model and Wind Data

The dispersion estimates for INEEL are based on the MDIFFH puff model model described by Sagendorf et al. (2001). MDIFFH is a specialized version of the MDIFF model used for operational dispersion support at INEEL. Both of these models represent pollutant dispersion as a series of puffs that grow and move independently as the wind field varies in space and time. The transport wind for each puff is computed using inverse-distance-squared interpolation among the available wind measurements.

INEEL wind measurements come from a tower network operated by FRD. This network is often called the INEEL Mesonet, or simply the Mesonet for brevity. The current incarnation of the Mesonet has been in operation since April 1993. Its core has consisted of approximately 30–35 meteorological towers maintained by FRD. Fig. 2 shows the locations of most FRD towers at the end of 2000. The tower density is highest within the INEEL boundaries, but a significant number of towers are present across the Snake River Plain. Since 1993 there have been a few additions and deletions of towers, but Fig. 2 is largely representative of what was available from 1993 until the end of 2001. The INEEL Mesonet also uses data feeds from towers operated by other agencies, but these are not used in dispersion modeling because of their infrequent reporting intervals and questionable quality control procedures.

The FRD Mesonet towers collect five-minute-average data, which are transmitted back to FRD for archiving in near real time. Most of them measure wind speed, direction, and the wind direction standard deviation at 15 m AGL. Temperature is typically sampled at 2 and 15 m AGL. Relative humidity is also sampled at 2 m. Three of the towers are taller. They have two levels of wind measurements, one at 10 m AGL and a second in the 46–76 m range. Once the data are transmitted to FRD, they go through several quality-control procedures before final archiving.

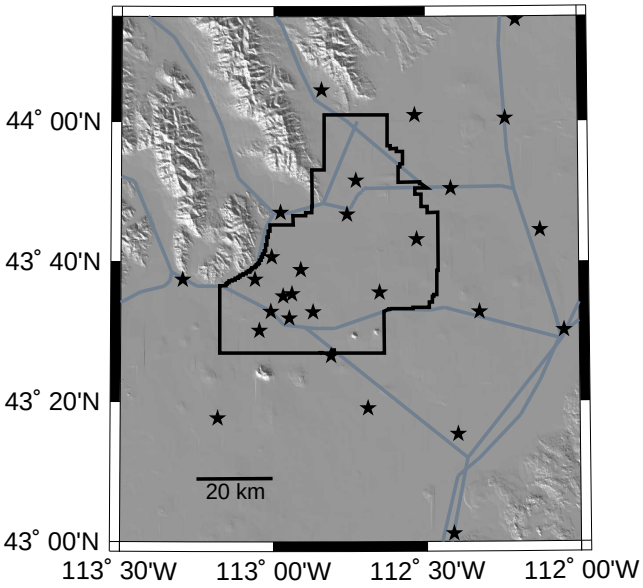

Figure 2: Map showing the locations of meteorological towers in the INEEL Mesonet. The towers are indicated by stars. The INEEL boundary is shown by heavy black lines. The gray lines are major roads. Five additional towers are just beyond the map domain.

The MDIFF model is intended for near real-time use during emergencies at INEEL. It can directly ingest the five-minute-average data available from the Mesonet. The MDIFFH model used here is based on the same transport and dispersion algorithms as MDIFF, but it uses hour-average rather than 5-minute-average data. It is mainly intended for planning scenarios and evaluating long-term dispersion. The hour-average data required for MDIFFH is computed from the five-minute-average Mesonet data. Neither of the models currently allows for deposition of material to the ground. The general algorithms used for MDIFF and MDIFFH can be found in Sagendorf et al. (2001).

A few minor modifications were made to MDIFFH for the study in this report. Most of these are related to the model's output variables. The most basic output variable reported by MDIFFH is the total integrated concentration ψ_m at each model grid point. However, the model also reports the travel time and travel distance of the first puff to reach each grid point during the simulation. Of course, many puffs can pass each grid point over the course of a simulation, so the travel time and distance of the first puff may not have much significance. The model was therefore modified to report a ψ_m-weighted travel time and travel distance based on all the puffs that reach each grid point. Each puff is weighted according to its relative contribution to ψ_m at the grid point.

MDIFFH was also modified to report the plume exposure time T_e, representing the total length of time the plume was present at each grid point during the simulation. During a model time step, a puff will contribute to ψ_m at a grid point only if the puff's concentration exceeds a minimum threshold χ_{min}. (This is done to save computational effort on puffs

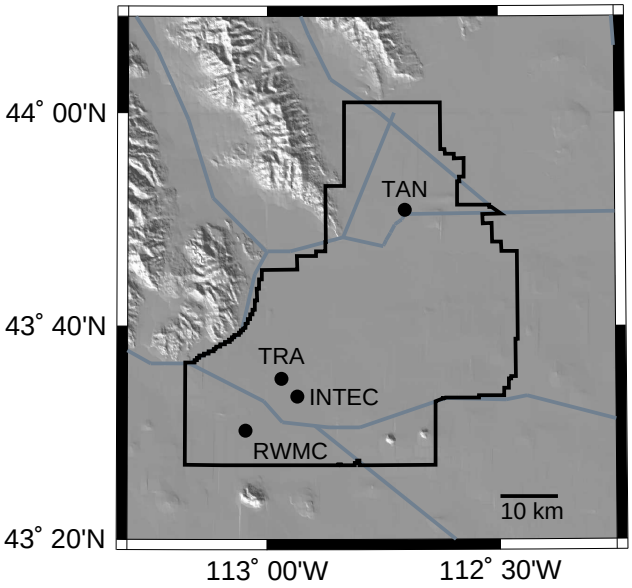

Figure 3: Locations of the four release locations considered in this study.

that are either highly diluted or distant from the grid point.) Hence, the grid point is exposed to the model plume any time at least one puff produces a concentration that exceeds χ_{min}. T_e is useful in determining whether worst-case ψ_m/Q values are related to high concentrations over short exposure times or to lower concentrations over longer exposure times. It can also be compared with the release time t_r.

3.2. Release Scenarios

INEEL has requested worst-case dispersion estimates at four INEEL facilities: the Idaho Nuclear Technology and Engineering Center (INTEC), the Radioactive Waste Management Complex (RWMC), Test Area North (TAN), and the Test Reactor Area (TRA). The locations of these facilities are shown in Fig. 3. INEEL requested surface-release scenarios at all four facilities and elevated-release scenarios at INTEC and TRA.

In Sagendorf (1996), short-range diffusion out to 15–20 km from the source was modeled using a 70×70 grid with a 500 m spacing. He also modeled longer range dispersion from INTEC and TRA using a 100×100 grid with a 2 km spacing. A similar approach is used here. In all, ten different release scenarios were considered, as shown in Table 1.

The 500 m grid used in the short-range scenarios had dimensions of 70×70, and it was centered at the release point. The 2 km grid used for the longer-range scenarios had dimensions of 60×70. This is smaller than the grid used by Sagendorf (1996), but restricts the model domain to a region where there is a reasonable density of Mesonet towers. This larger domain was centered at a fixed point (latitude 43.64° N, longitude 112.73° W) on the eastern side of INEEL for both the INTEC and TRA scenarios.

Table 1: Source configuration and model grid spacing for the ten release scenarios.

Release				Grid
Scenario	Location	duration (h)	elevation (m AGL)	spacing (km)
1	INTEC	1.0	0	0.5
2	INTEC	1.0	76	0.5
3	INTEC	1.0	0	2.0
4	INTEC	1.0	76	2.0
5	RWMC	1.0	0	0.5
6	TAN	1.0	0	0.5
7	TRA	2.5	0	0.5
8	TRA	2.5	61	0.5
9	TRA	2.5	0	2.0
10	TRA	2.5	61	2.0

The release durations in Table 1 are 2.5 h for TRA and 1 h for the other facilities. These are consistent with Sagendorf (1996), and are related to the accident scenarios at the facilities. Likewise, the release elevations for the stack releases are consistent with Sagendorf. For all the scenarios, the source release rate q was fixed at 1 unit (Ci, kg, *etc.*) per hour. The total material released was therefore 2.5 units for the TRA scenarios and 1 unit for the others.

3.3. Model Runs

Consistent data from the INEEL Mesonet are available starting 1 April 1993. For each release scenario in Table 1, a separate MDIFFH run was started every hour during the period from 1 April 1993 to 31 December 2001. This provides a maximum of 76728 total model runs for each scenario. However, in the early years there were limited periods when MDIFFH was unable to run because of missing Mesonet data. Release scenario 9 had the greatest number of lost hours at 354, but this still represents less than 1% of the maximum.

At the end of each run, MDIFFH saved the value of ψ at each grid point in the model domain. It also saved some ancillary variables such as the ψ-weighted puff travel time and travel distance at each grid point. When all the hourly runs were completed for a particular scenario, there were over 76000 separate values of ψ at each grid point. These values were used to compute the pdfs $p(\psi_m/Q \,|\, r, D, I_m)$ and $p(\psi_m/Q \,|\, r, D, I_m, H)$ together with the probability $P(H \,|\, r, D, I_m)$ of a plume hit. Of course, the model uses a rectangular grid, so the model results are actually given in rectangular coordinates (x, y) rather than (r, D).

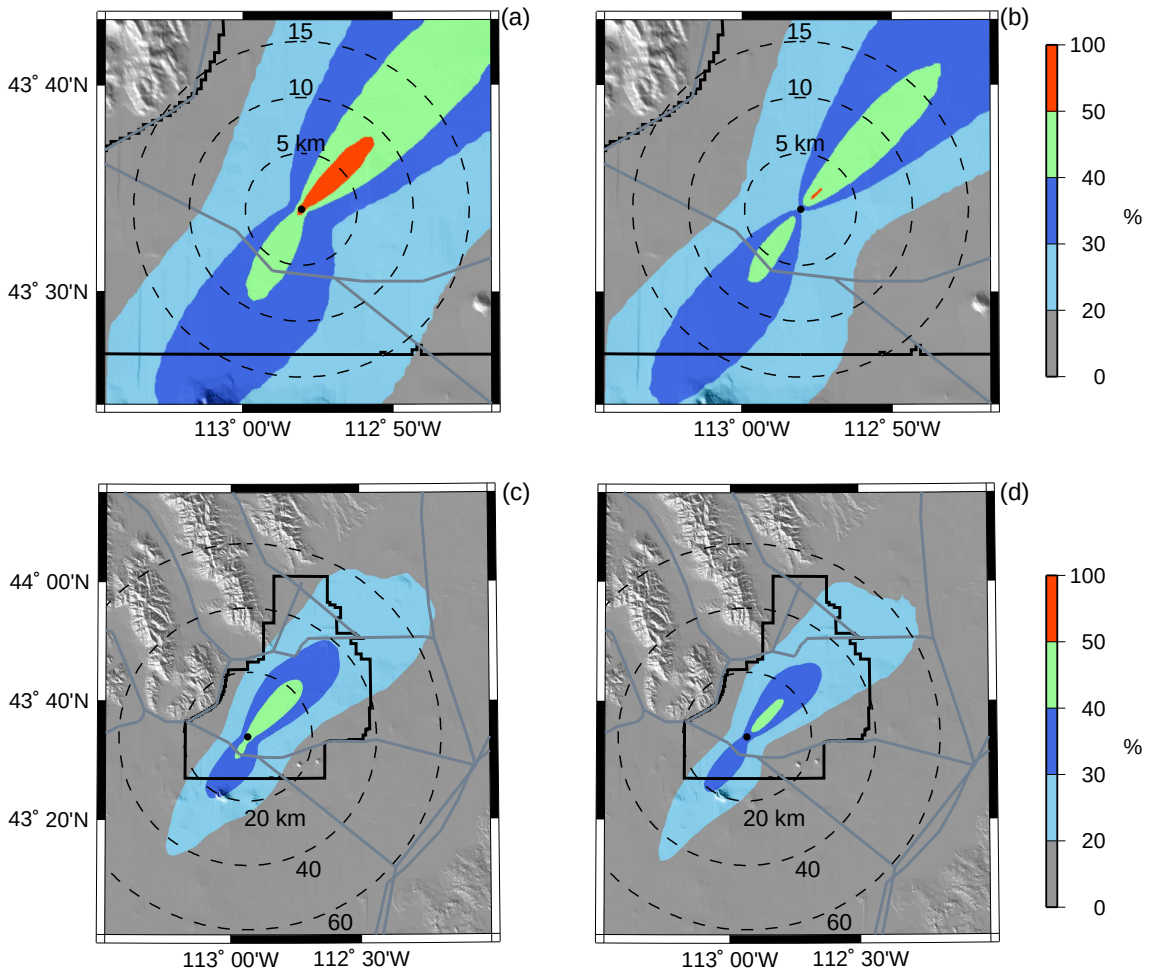

Figure 4: Percentage of plume hits for the INTEC release configurations. (a) surface release, 500 m grid; (b) stack release, 500 m grid; (c) surface release, 2 km grid; (d) stack release, 2 km grid.

4. Modeling Results

4.1. Probability of a Plume Hit

Section 2 demonstrated that one of the issues of relevance to dispersion risk assessment is the probability $P(H \mid r, D, I_m)$ of a plume hit at a fixed location (r, D). Figure 4 shows the MDIFFH estimates of this probability for all the INTEC release configurations. For a surface release, this figure shows that only a small region to the northeast of the source has greater than a 50% probability of a hit. This is the only region where the median value of $p(\psi_m/Q \mid r, D, I_m)$ is nonzero.

The favored southwest-northeast channeling of the wind is also clearly evident in the figure. This channeling is due partly to the general orientation of the Eastern Snake River Plain and partly to local topography. As stated in the Introduction, the plain is oriented southwest to northeast, with generally higher elevations toward the northeast. Several

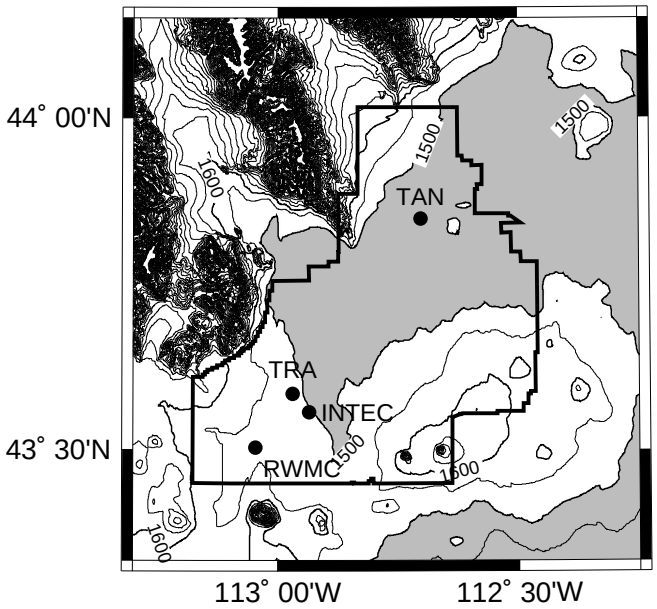

Figure 5: Terrain contours near INEEL at 50 m intervals. Elevations below 1500 m MSL are shaded in light gray.

channeling mechanisms (see Whiteman and Doran 1993; Eckman 1998) based on synoptic pressure gradients and differential heating will cause the near-surface wind to align with the plain's southwest-northeast axis. This regional channeling is sometimes overridden, however, by local topographic effects. At INEEL, a shallow depression protrudes into the site as shown in Fig. 5. Wendell (1972) and Clawson et al. (1989) have shown that this depression has significant effects on the observed winds.

INTEC is on the southern boundary of the shallow depression. The local terrain has a northeast aspect, opposite to the overall aspect of the Snake River Plain. Nighttime wind measurements from a tower near INTEC have sometimes shown a shallow southwesterly drainage along the local slope overlaid by a regional northeasterly drainage associated with the Snake River Plain (Clawson et al. 1989). Hence, the local terrain slope may be partly responsible for the higher percentages of plume hits to the northeast of INTEC in Fig. 4.

As one would expect, the elevated releases in Fig. 4 have lower percentages, but the general shape of the contours is similar to the surface releases. At longer distances from the source, the differences between the surface and elevated releases become less significant. By the time the puffs reach these distances, they are usually well-mixed in the vertical, so the release height is not a factor unless it is so large that the puffs remain above the boundary layer.

The plume hits for the RWMC and TAN scenarios are displayed in Fig. 6. RWMC shows northeast-southwest channeling like INTEC, but the probability of southwesterly plume transport is much lower. This facility is further removed from the shallow depression that occupies much of the northern end of INEEL, and it is also located in a gully with higher

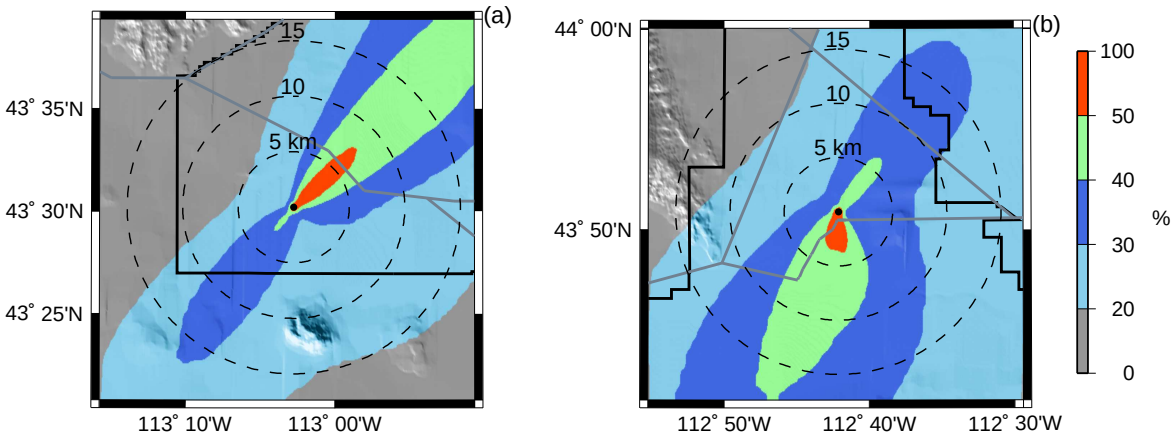

Figure 6: Percentage plume hits for the (a) RWMC and (b) TAN release configurations.

terrain to the north, west, and south (Fig. 5). This local topography appears to suppress the development of northeasterly winds at RWMC.

The TAN contours in Fig. 6 show a strong preponderance of southerly and southwesterly plume transport. This facility often experiences northerly winds channeled within the shallow terrain depression (Wendell 1972). In addition, the mouth of a large tributary valley (Birch Creek) is located just to the northwest of TAN. Clawson et al. (1989) noted that flows exiting this valley often reach TAN as north-northwest winds. There is still a significant probability of northeasterly plume transport in Fig. 6, representing periods when the regional winds overcome the local topography.

Figure 7 shows the TRA plume-hit percentages for the different release configurations. TRA is close to INTEC, so the contours for these two release points have similar shapes. However, the TRA contours cover a significantly larger area because each TRA release lasted 2.5 hours rather than 1 hour (Table 1).

4.2. 95th Percentiles for All Releases

As stated in Section 2, one of the parameters that can be taken to represent worst-case dispersion is the 95th percentile A_{95} of the pdf $p(\psi_m/Q \,|\, r, D, I_m)$. This pdf is not conditional on a plume hit occurring, so all the null concentrations representing plume misses are included in this distribution. From this point forward, only the surface releases in Table 1 are discussed. The results from the elevated releases look similar to those from the corresponding surface releases, except that the A_{95} (or C_{95}) values are systematically lower.

Figure 8 shows the A_{95} contours for the surface releases from all four facilities. These are all based on the higher-resolution 500 m MDIFFH grids. INTEC and TRA have contours of similar shape. Their contours above 10^{-6} s m^{-3} are nearly symmetric about the release

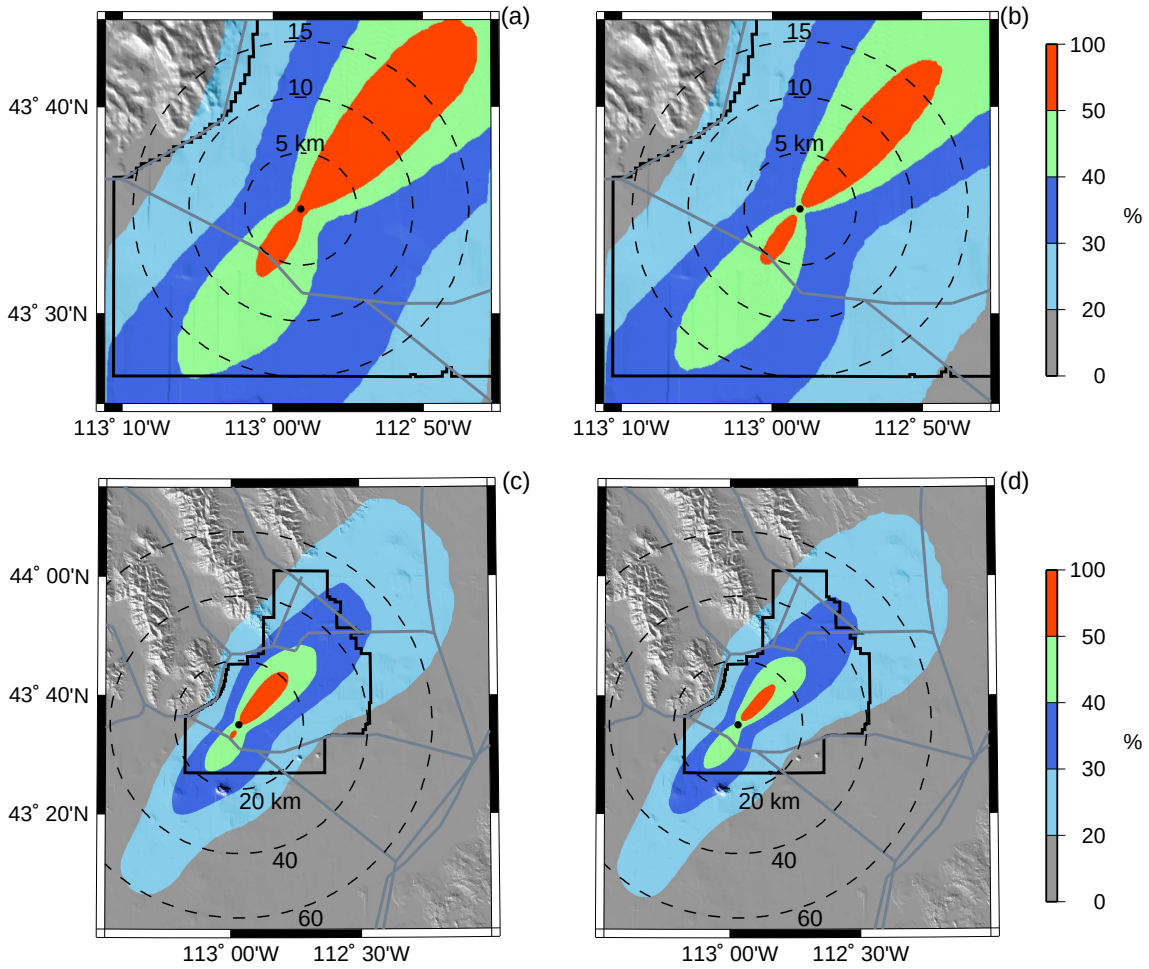

Figure 7: Percentage of plume hits for the TRA release configurations. (a) surface release, 500 m grid; (b) stack release, 500 m grid; (c) surface release, 2 km grid; (d) stack release, 2 km grid.

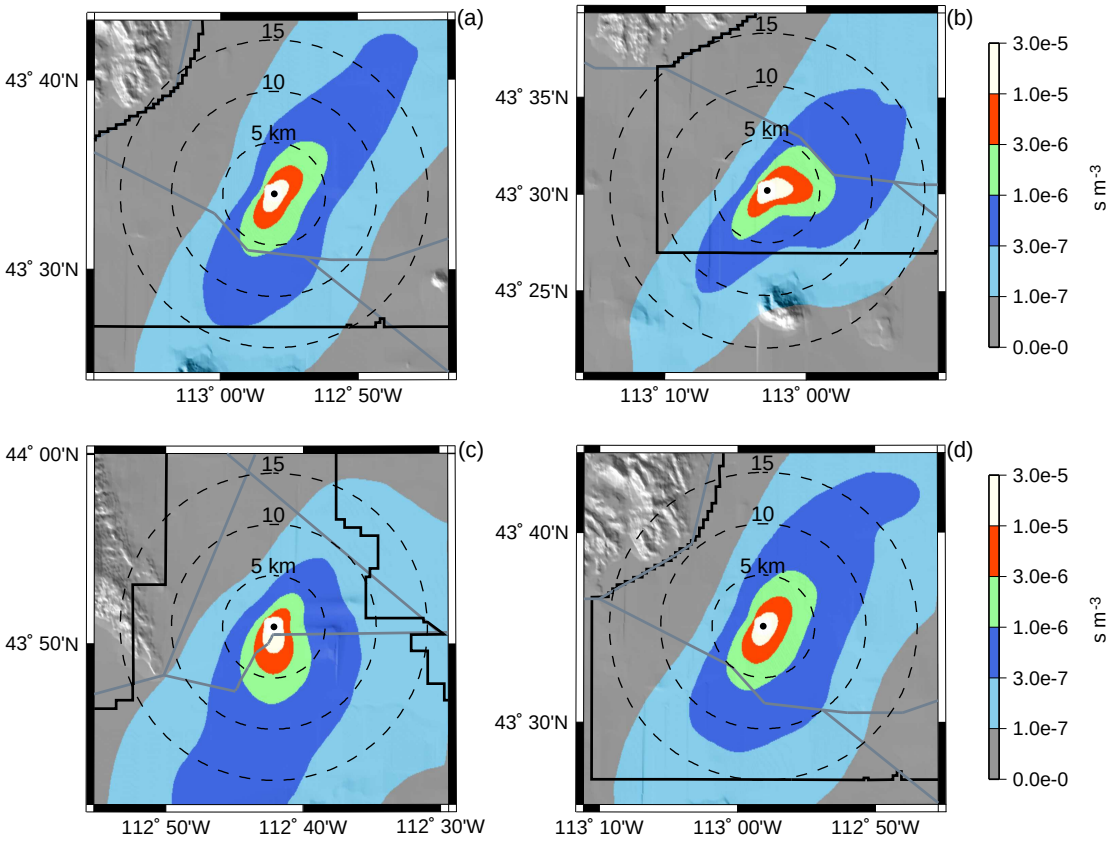

Figure 8: Contours of A_{95} in $\mathrm{s\,m^{-3}}$ for the surface-release configurations using a 500 m grid. (a) INTEC; (b) RWMC; (c) TAN; (d) TRA.

point, and are elongated along a northeast-southwest axis. Another way of looking at this result is that the worst-case events that extend furthest downwind from these facilities can be associated with either northeasterly or southwesterly winds.

At RWMC there is one region of high A_{95} values extending to the southwest of the source and another extending to the east. The high values to the southwest appear to be similar in nature to those observed at INTEC and TRA. At all three facilities, these values are likely associated with a regional northeasterly (and probably stable) flow within the Snake River Plain. The high A_{95} values extending to the east of RWMC are not as expected. Figure 6 shows that easterly plume transport at RWMC is not a regular event. However, the 30% contour in Fig. 6 does have somewhat of a bulge out to the east. This suggests there are relatively infrequent periods when the wind at RWMC comes from the west, but these periods have a disproportionate presence in the worst-case dispersion events. In Fig. 5, a shallow gully extends to the west-northwest of RWMC. This is actually the bed of the Big Lost River, which comes out of a tributary valley that feeds into the Snake River Plain. It therefore seems plausible that the worst-case events with westerly winds may represent drainage winds moving along the Big Lost River.

For TAN most of the highest A_{95} values are associated with northerly or northeasterly

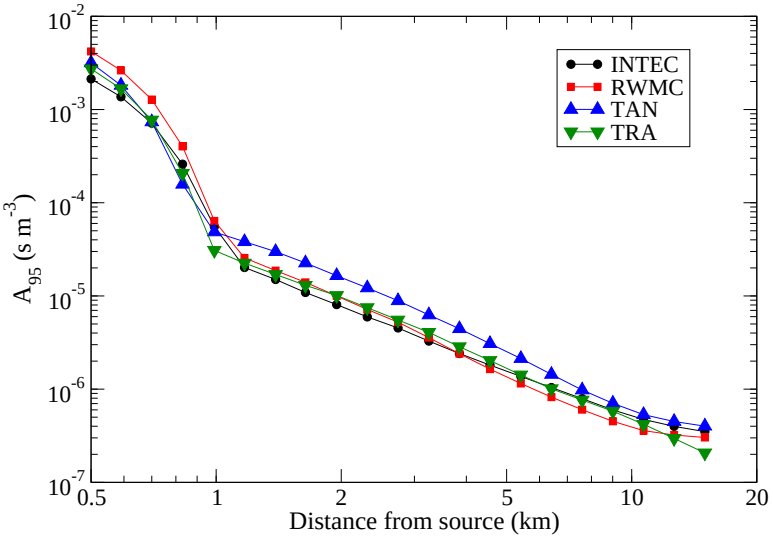

Figure 9: Variation of A_{95} with distance from source for selected directions D. The directions are 45° for INTEC, 60° for RWMC, 180° for TAN, and 195° for TRA. These were chosen visually by considering the elongation of the contours out to about 15 km in Fig. 8.

winds within the shallow depression. The local topography therefore appears to dominate the worst-case events at this facility.

The contours in Fig. 8 show that some directions D from the source have higher A_{95} values than others. Figure 9 shows how A_{95} decreases with distance along selected directions from each release location. These were selected from Fig. 8 by visually locating which directions have the highest A_{95} values out to about 15 km. Although the direction selection was somewhat subjective, the curves in Fig. 9 are remarkably consistent. They all show a steep slope out to 1 km, and a shallower slope thereafter. The horizontal puff growth rate in MDIFFH does not change until the puffs travel 20 km (Sagendorf et al. 2001), so the change in slope at 1 km is likely due to the vertical diffusion algorithm. MDIFFH changes the vertical growth rate when the puff becomes well-mixed vertically. Hence, the change in slope at 1 km may represent the typical distance at which the puffs become well mixed under the worst-case conditions.

Figure 10 shows the A_{95} contours for INTEC and TRA based on the larger 2 km grid. The channeling of the wind by the Snake River Plain is still the dominant influence at these longer ranges. The contours tend to extend furthest from the source to the northeast, so the worst-case events with the greatest potential to affect more distant locations are associated with southwesterly winds. One note of caution with the large domain in Fig. 10 is that the shape of the outermost contours may partly be due to model artifacts. MDIFFH drops puffs that are more than 20 km from any meteorological tower, so the contours in the large domain may to some extent be a reflection of the tower density in Fig. 2.

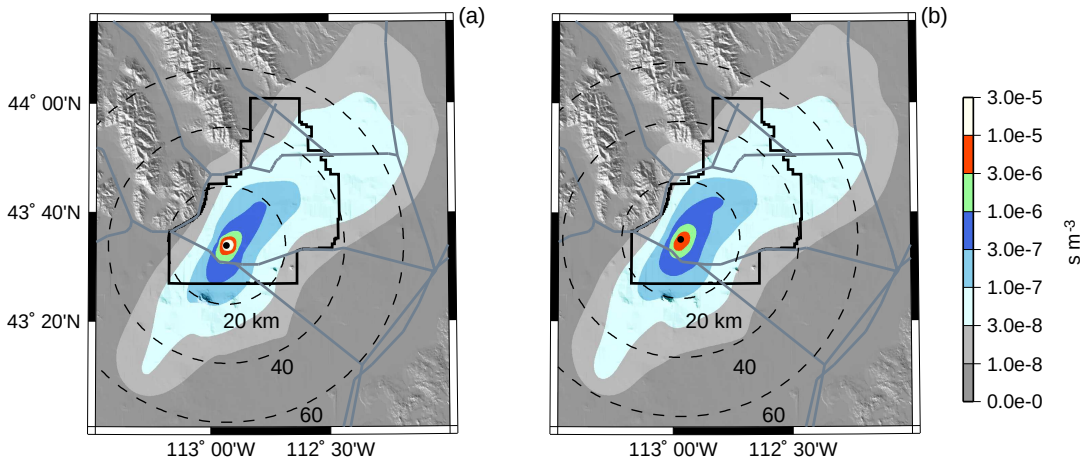

Figure 10: Contours of A_{95} for the (a) INTEC and (b) TRA release configurations using the 2 km grid.

4.3. 95th Percentiles for Plume Hits

The percentile plots shown in the last subsection were based on all the available model runs for a particular release scenario. Here, we focus on subsets of runs where a plume hit has occurred at the location $(r.D)$. The pdf for these subsets is $p(\psi_m/Q \,|\, r, D, I_m, H)$, and the 95th percentile is denoted by C_{95}. This percentile will always be larger than or equal to A_{95}. We also consider the median C_{50} of this pdf.

Figure 11 shows the C_{95} values on the 500 m model grids. The transport wind direction is less of a factor for the upper tail of $p(\psi_m/Q \,|\, r, D, I_m, H)$, because of the restriction to cases where a plume hit has occurred. This explains why the C_{95} contours are more circular than the A_{95} contours in Fig. 8. However, the effects of the wind direction are not completely eliminated in C_{95}. At some locations, the C_{95} value results from a direct hit by the plume centerline, whereas at other locations the C_{95} value results from only a grazing hit by the outer fringes of the plume. In Fig. 11 the remaining wind-direction effects become more of a factor at greater distances from the sources.

Out to about 10 km from the source, a northerly transport wind gives the highest C_{95} values at INTEC, TAN, and TRA. These are all consistent with a regional drainage flow moving down the Snake River Plain. At RWMC a westerly wind gives the highest values. As discussed earlier, this flow direction appears to be associated with drainage along the bed of the Big Lost River. This drainage is not all that frequent throughout the year, but it appears to be significant for worst-case dispersion scenarios at RWMC.

As with A_{95} in Fig. 9, we can consider how C_{95} varies with distance from the source along selected bearings. Figure 12 shows the results. At distances less than 1 km from the source. the C_{95} values in Fig. 12 are roughly the same as the A_{95} in Fig. 9. At larger distances, C_{95} tends to be a factor of 2–7 larger.

The median values C_{50} for the surface releases are shown in Fig. 13. They are of course

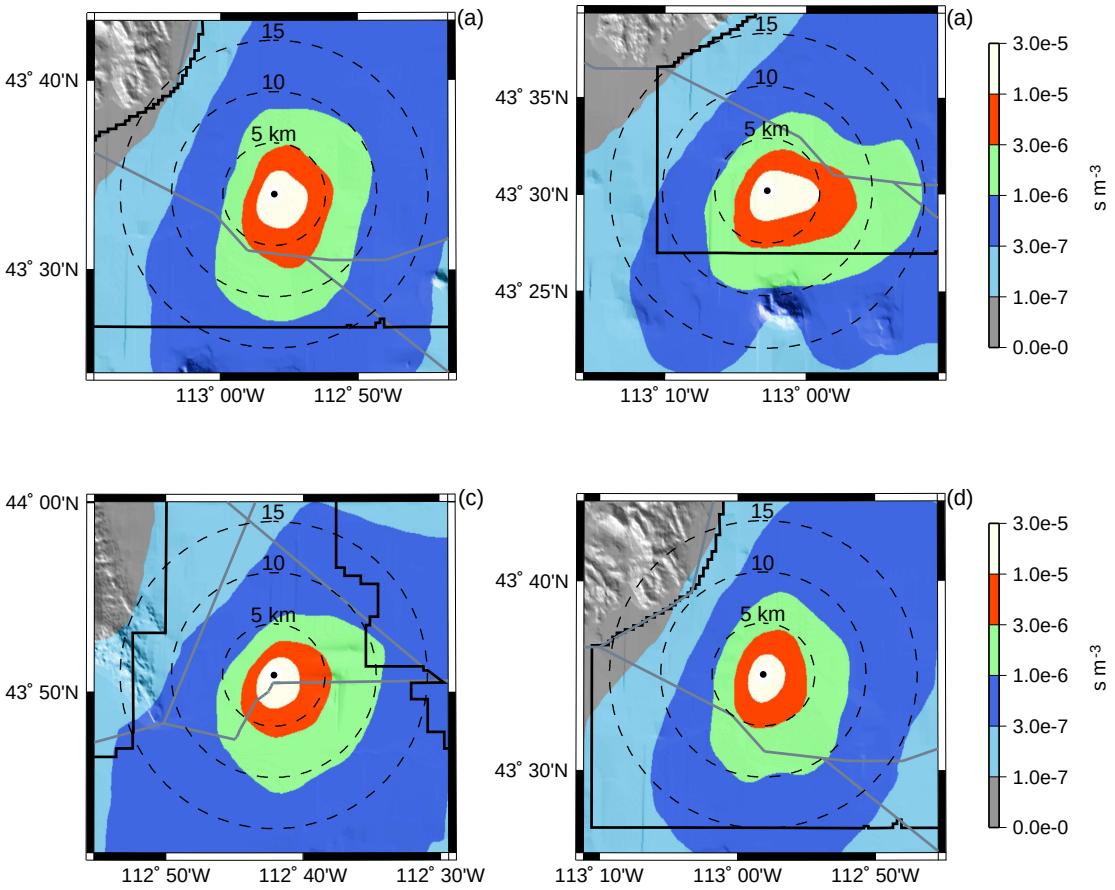

Figure 11: Contours of C_{95} in sm^{-3} for the surface-release configurations using a 500m grid. (a) INTEC; (b) RWMC; (c) TAN; (d) TRA.

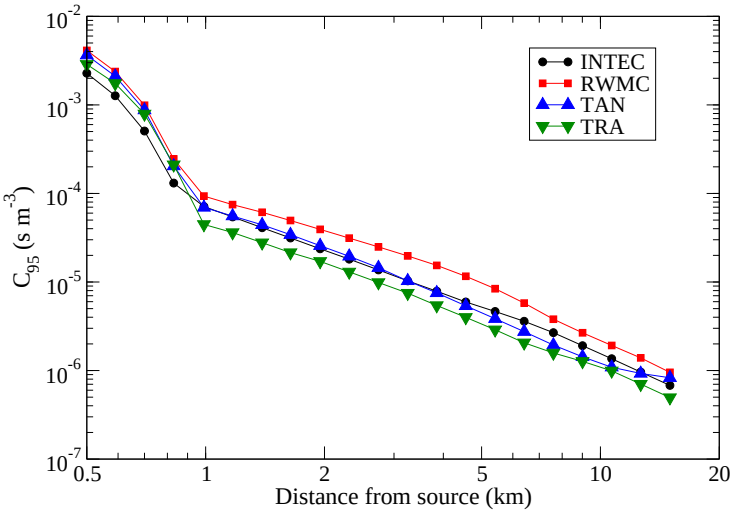

Figure 12: Variation of C_{95} with distance from source for selected bearings. The bearings are 175° for INTEC, 95° for RWMC, 175° for TAN, and 190° for TRA. These were chosen visually by considering the elongation of the contours out to about 15 km in Fig. 11.

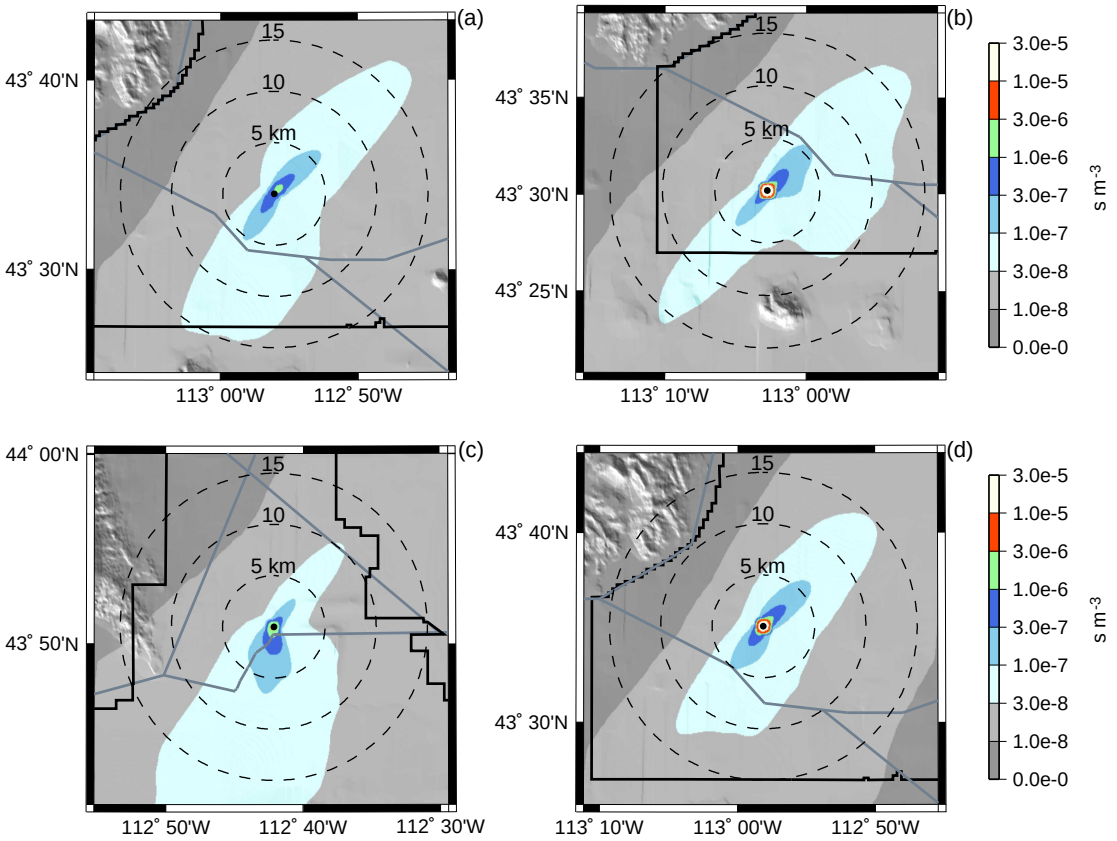

Figure 13: Contours of C_{50} in sm^{-3} for the surface-release configurations using a 500m grid. (a) INTEC; (b) RWMC; (c) TAN; (d) TRA.

much lower than the C_{95} values. It is clear that the median of C_{50} is more strongly affected by the transport wind direction than C_{95}. Overall, the contours in Fig. 13 are similar in shape to the A_{95} contours in Fig. 8.

The C_{95} and C_{50} results for the large model domain are shown in Fig. 14. The lowest contours for C_{95} more or less follow the outline of the Snake River Plain. Hence, nearly any location on the plain has a nominal risk of exposure to a plume emitted from INEEL. The lack of contours in the southwestern corner of these plots is an artifact due to a lack of meteorological towers in this region. As mentioned earlier, MDIFFH drops puff more than 20 km from any tower.

The areas outside the INEEL boundary with the highest C_{95} values tend to be to the northeast of the sources. This is nearly opposite of what was found at near-field ranges up to about 10km from the source (Fig. 11), where the highest values were south of the source. The explanation for this is that the near-field results are probably dominated by light-wind events. These light winds are not persistent enough to transport the puffs over long ranges, so the far-field results are determined more by events with higher wind speeds. Generally, the higher wind speed events in the Snake River Plain are from the southwest.

Figure 14 suggests that areas to the southeast of INEEL may be exposed to higher

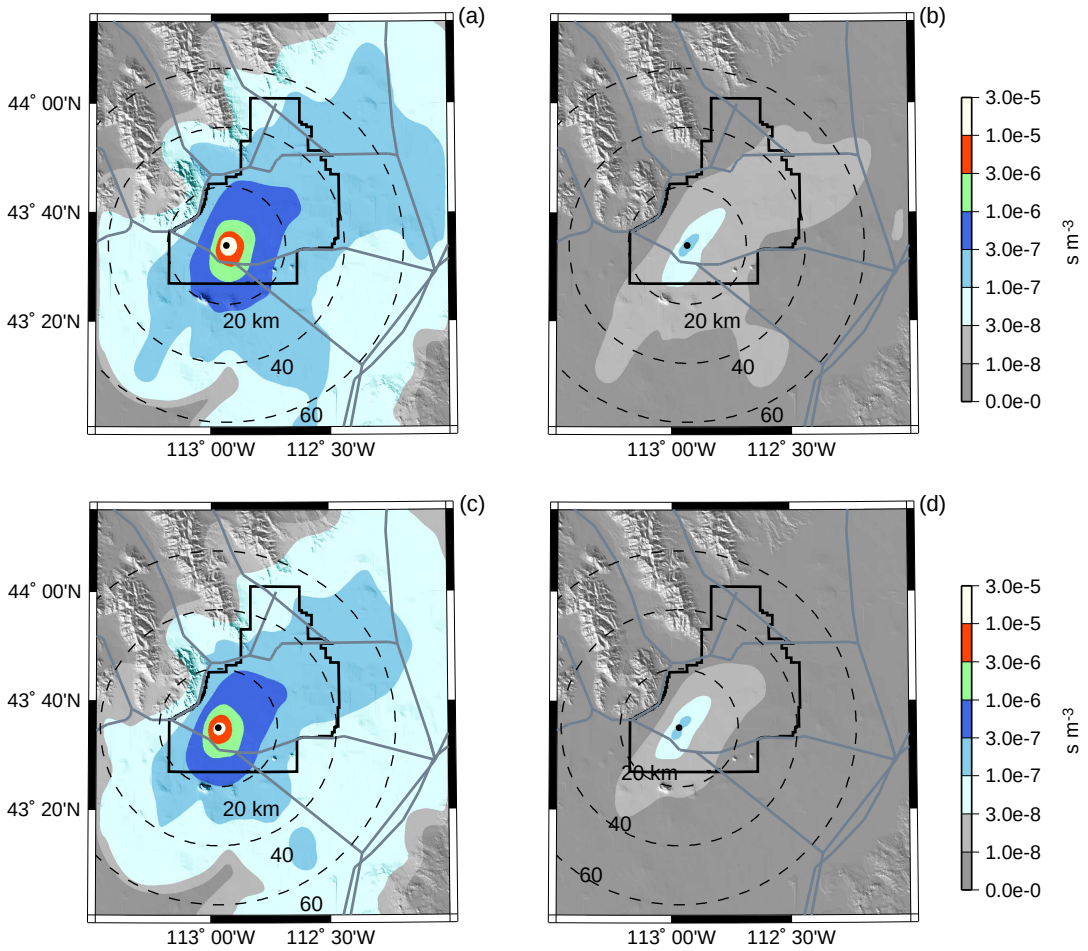

Figure 14: Contours of C_{95} and C_{50} for the large model domain. (a) INTEC C_{95}; (b) INTEC C_{50}; (c) TRA C_{95}; (d) TRA C_{50}.

concentrations. There is some suspicion, however, that this is another model artifact related to tower location rather than flow channeling. This region of higher C_{95} values may just be following the chain of towers that extends to the southeast in Fig. 2. Despite this possible artifact, both the C_{95} and C_{50} contours suggest that material released from INTEC has a greater chance of moving east across the valley than material released from TRA. This is rather surprising given the close proximity of the two facilities (Fig. 3).

5. Conclusions

The concept of worst-case dispersion is relatively simple on an abstract level. It relates to a set of atmospheric conditions producing the highest pollutant concentrations at some point of interest. If there is a desire to go beyond the abstractions and develop quantitative estimates, a more rigorous definition of worst-case dispersion is required. This report demonstrated, however, that there are many possible definitions, none of them being

applicable to all situations. The concentration χ (or total integrated concentration ψ) at a specific receptor location always has some level of uncertainty that is representable as a probability density function (pdf). The worst-case dispersion should therefore be defined statistically, and it logically should have some relevance to the the upper tail of the pdf. One obvious choice is the 95th percentile of the pdf.

Even if it is agreed to use a 95th percentile for the worst-case, there is the problem that many different pdfs can be chosen for χ or ψ. Einerson (1994) based the worst-case estimates for INEEL facilities on a pdf that considers the concentration only along the plume centerline. This pdf has just one space dimension in the sense that its only spatial variable is the distance downwind x_c along the plume centerline. Sagendorf (1996) used quite different pdfs that are functions of both the range r and direction D from the source. The Sagendorf and Einerson 95th percentiles are not directly comparable since they come from different pdfs. This appears to have been overlooked at INEEL (e.g. Bonney 1997), where the prevailing explanation is that the Sagendorf and Einerson differences are due only to differing models (puff model versus straight-line Gaussian plume).

This study considered two different pdfs for the analysis of worst-case dispersion. Like Sagendorf (1996), they are a function of a receptor's range r and direction D from the source. Both pdfs were generated by making repeated runs of the MDIFFH puff model based on nearly nine years of data from the INEEL Mesonet. The first pdf $p(\psi_m/Q \,|\, r, D, I_m)$ represents the probability of the model producing a ratio ψ_m/Q given no restrictions on time, date, or meteorological conditions. The 95th percentile for this pdf is A_{95}. Since this distribution contains many null values representing cases when the plume misses the receptor location, a second pdf $p(\psi/Q \,|\, r, D, I, H)$ was defined. It is conditional on the assumption H that the model plume hit the receptor location at some point during the model run. This pdf represents a restricted set of meteorological conditions which allow the plume to reach the receptor. The 95th percentile for this pdf is C_{95}.

The A_{95} contours for INTEC and TRA tended to be highest to the northeast and southwest of the sources, which is related to wind channeling within the Snake River Plain. At RWMC and TAN, the A_{95} values are affected by flows coming from nearby valleys that feed into the Snake River Plain. The C_{95} contours for all the release locations tended to be more symmetrically distributed about the source. This is explained by the additional condition H, which diminishes the effect of the wind direction on the integrated concentration. Beyond about 1 km from the source, the C_{95} values tend to be a factor of 2–7 larger than the A_{95} values.

One problem shared by Einerson (1994), Sagendorf (1996), and this study is that all the worst-case statistics are based on model estimates ψ_m without any consideration of how ψ_m relates to the actual integrated concentrations ψ expected at the receptor locations. As shown by Eq. (9), the pdfs for ψ_m and ψ are related through a third pdf representing the model uncertainty. In concept, the model uncertainty can be evaluated using existing model performance data together with something like a maximum entropy approach. Unfortunately, this was beyond the limited scope of this study. The consequence of neglecting the uncertainty is that the worst-case statistics reported here come from model

pdfs for ψ_m that are likely narrower than the corresponding pdfs for the actual integrated concentration ψ.

The A_{95} and C_{95} values reported here represent two different definitions of worst-case dispersion for the INEEL facilities. Einerson (1994) provided a third possible definition. One might ask which of these should be used for INEEL consequence assessment. This moves outside of the meteorological arena and more into the areas of policy and decision making. The decision makers need to determine which definition of worst-case dispersion best suits the issues that are being addressed.

Acknowledgments

This work was sponsored under an agreement between FRD and Bechtel BWXT Idaho, LLC., who operates INEEL for the U.S. Department of Energy. The image in Fig. 1 was provided by Doug Walker of the State of Idaho's INEEL Oversight Program.

References

Anderson, J. E., K. T. Ruppel, J. M. Glennon, K. E. Holte, and R. C. Rope, 1996: Plant communities, ethnoecology, and flora of the Idaho National Engineering Laboratory. Report ESRF-005, Environmental Science Research Foundation, Idaho Falls, Idaho, 111 pp.

Bonney, R. F., 1997: Evaluation and application of NOAA atmospheric dispersion parameters for consequence assessment calculations. Interdepartmental Communication RFB-001-97, Lockheed Martin Idaho Technologies Company, Idaho Falls, Idaho, 17 pp.

Bretthorst, G. L., 1996: An introduction to model selection using probability theory as logic. In *Maximum Entropy and Bayesian Methods*, G. R. Heidbreder, ed., Kluwer Academic Publishers, 1–42.

Clawson, K. L., G. E. Start, and N. R. Ricks, 1989: Climatography of the Idaho National Engineering Laboratory, 2nd edition. Report DOE/ID-12118, U. S. Department of Energy, Idaho Operations Office, Idaho Falls, Idaho, 155 pp.

Eckman, R. M., 1998: Observations and numerical simulations of winds within a broad forested valley. *J. Appl. Meteor.*, **37**, 206–219.

Einerson, J. J., 1994: Air dispersion parameters for use in Idaho National Engineering Laboratory Department of Energy safety analysis. Report EGG-WM-11243, EG&G Idaho, Idaho National Engineering Laboratory, Idaho Falls, Idaho, 45 pp.

Jaynes, E. T., 1957: Information theory and statistical mechanics. *Phys. Rev.*, **106**, 620–630.

Sagendorf, J. F., 1996: Atmospheric transport and diffusion modeling for short term releases from INEL facilities. Internal Report ARLFRD 96-108, NOAA/ARL Field Research Division, Idaho Falls, Idaho, 50 pp.

Sagendorf, J. F., R. G. Carter, and K. L. Clawson, 2001: MDIFF transport and diffusion models. NOAA Technical Memorandum OAR ARL-238, NOAA Air Resources Laboratory, Silver Spring, Maryland, 26 pp.

Wendell, L. L., 1972: Mesoscale wind fields and transport estimates determined from a network of wind towers. *Mon. Wea. Rev.*, **100**, 565–578.

Wenzel, D. R. and B. J. Schrader, 2001: The Radiological Safety Analysis Computer Program (RSAC-6) user's manual. Technical Report INEEL/EXT-01-00549, Idaho National Engineering and Environmental Laboratory, Idaho Falls, Idaho, 267 pp.

Whiteman, C. D. and J. C. Doran, 1993: The relationship between overlying synoptic-scale flows and winds within a valley. *J. Appl. Meteor.*, **32**, 1669–1682.

Appendix: Ancillary Statistics

The statistics reported in the main body of the report are all associated with the total integrated concentration ψ. However, other aspects of the puff dispersion were also reported in the MDIFFH output, including the average travel time and travel distance of the puffs reaching each model grid point. These averages used a ψ weighting, in which the travel time and distance of each puff was weighted by its relative contribution to ψ. Statistics for the puff travel time and travel distance are provided in this appendix. They are useful for such issues as whether the pollutant is taking a direct path to reach a specific location or whether high ψ values are related to recirculating plumes within the Snake River Plain.

In presenting statistics for the travel time and distance, it is desirable to provide something that can be related to the 95th percentiles A_{95} and C_{95}. The simplest procedure would be to pick out the MDIFFH runs that happen to correspond to A_{95} and C_{95}, and then report the travel times and distances associated with these runs. This is arbitrary, however, because sorting the MDIFFH runs by ψ/Q does not imply that they are also sorted by travel time or any other variable.

An alternative approach was chosen in this study, based on the pdfs $p(\psi_m/Q \,|\, r, D, I_m)$ and $p(\psi_m/Q \,|\, r, D, I_m, H)$ that were used to define A_{95} and C_{95}. First, subsets of the MDIFFH runs falling within the top 10% of these pdfs were extracted. The median travel time and distance were then computed for these subsets. The intention with these statistics is to provide values representative of the top decile of the pdfs, thereby having some relevance to A_{95} and C_{95}. Medians could also be provided over the full pdfs, but these may not be relevant to the worst-case events at the upper tails. The median travel time and travel distance for the $p(\psi_m/Q \,|\, r, D, I_m)$ top decile are respectively denoted by τ_a and λ_a. Likewise, τ_c and λ_c apply to the top decile of $p(\psi_m/Q \,|\, r, D, I_m, H)$.

Figures 15 and 16 show contours of τ_a and τ_c for all four release locations. For τ_a the most rapid plume transport takes place along the northeast-southwest axis of the Snake River Plain. Within the first hour after release, the puffs can get out to about 8–10 km from the source along this axis. This corresponds to an advection speed of about 2.5 m s^{-1}. Along the northwest-southeast axis perpendicular to the plain, the τ_a values are significantly higher. This suggests that either the mean advection speed is lower, or that the puffs are taking an indirect path to reach these locations. The contours for τ_c are more circular than those for τ_a. However, the 1 h contour for τ_c does not get as far from the source, which suggests that the MDIFFH releases associated with τ_c tended to have lower advection speeds.

Figures 17 and 18 show contours for λ_a and λ_c. The λ_a contours to the southwest of the sources closely match the range circles, indicating that the plumes are traveling in nearly a straight line in this direction. The same is true to the northeast of the source out to about 10 km from the source. Beyond this distance, λ_a tends to be larger than the straight-line distance. At 15 km to the northeast of TRA, for example, the plume's travel distance is closer to 20 km. To the northwest and southeast of the sources, the λ_a values tend to be much larger than the straight-line distance from the source.

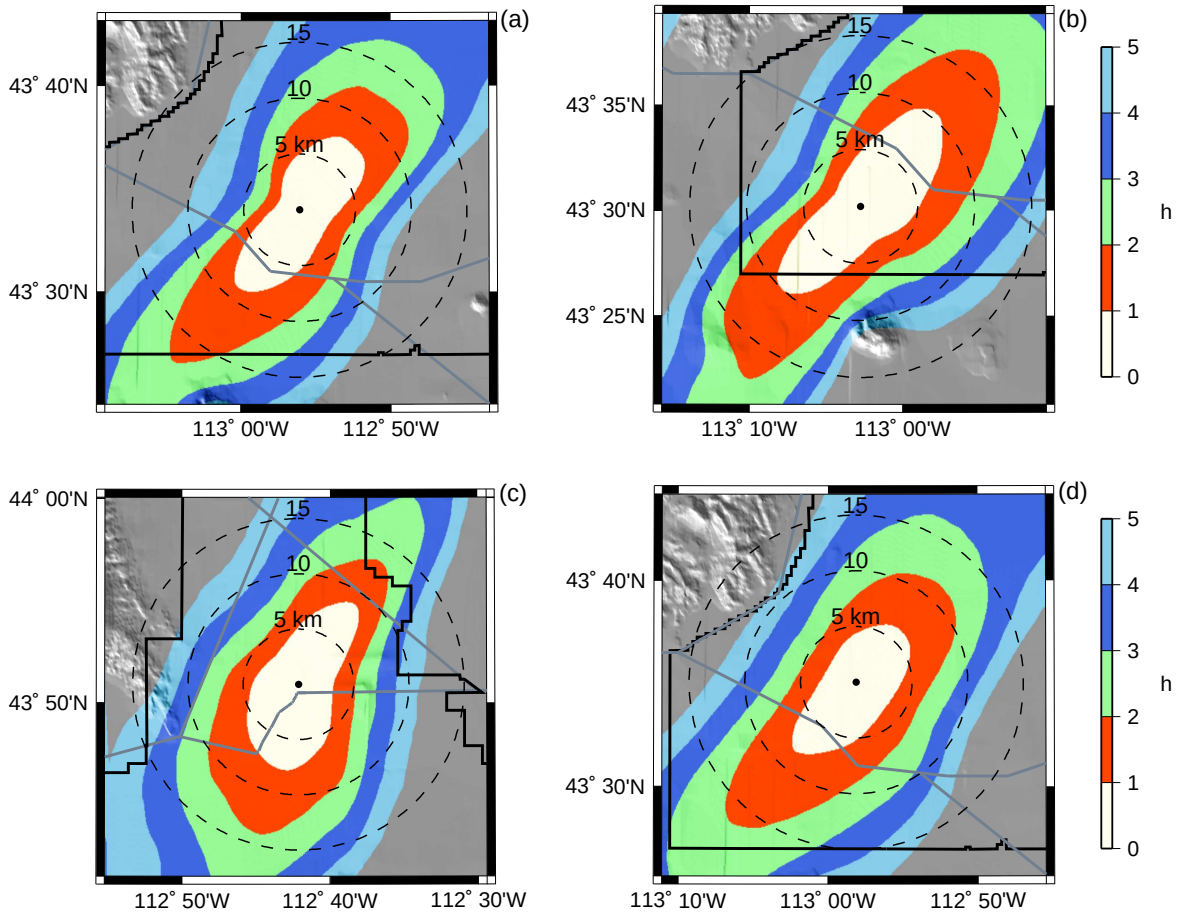

Figure 15: Contours of τ_a for surface releases from the four release locations. (a) INTEC; (b) RWMC; (c) TAN; (d) TRA.

The λ_c contours in Fig. 18 are more circular in shape. In fact, the 5 km contours closely match the 5 km range rings. The correspondence between the contours and range rings is not as good at larger distances. As with λ_a, the most persistent straight-line transport is associated with southwesterly directions from the source.

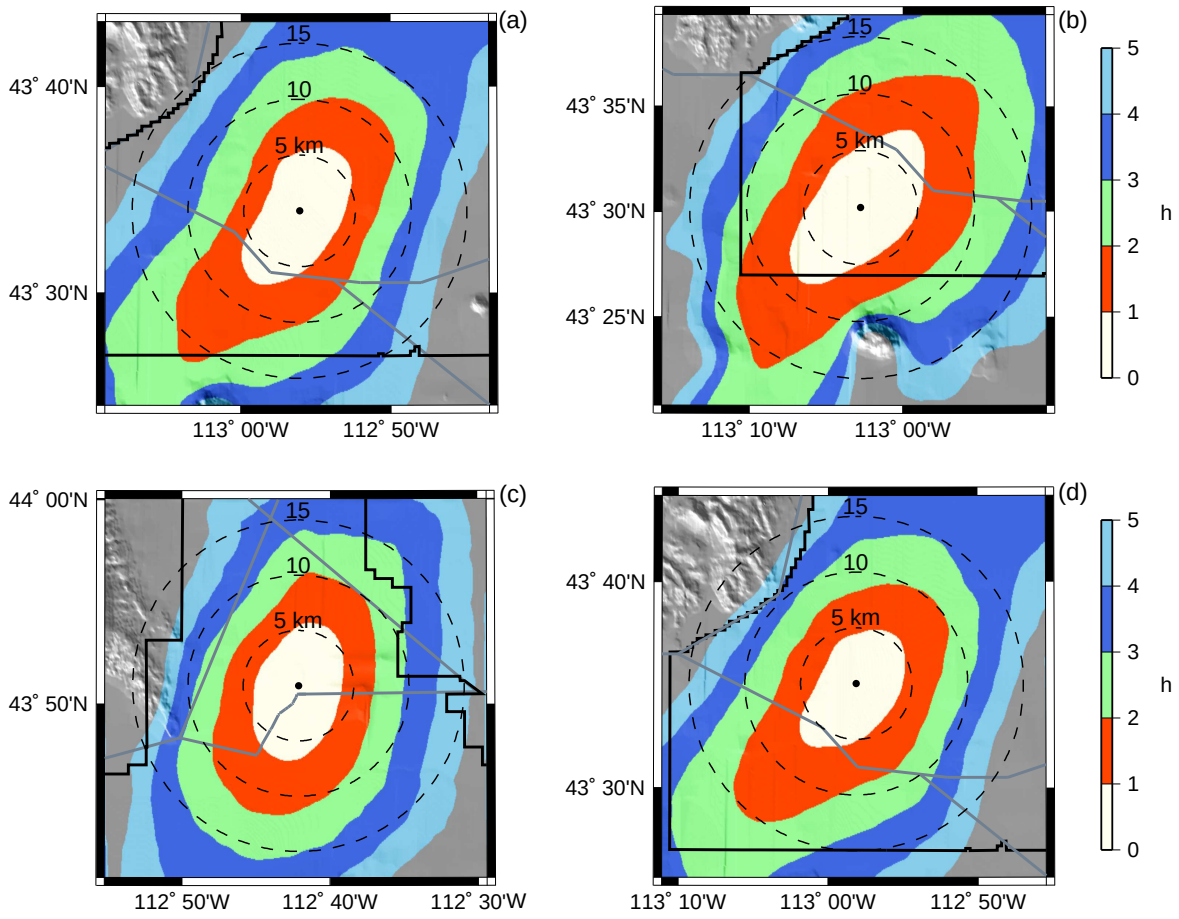

Figure 16: Contours of τ_c for surface releases from the four release locations. (a) INTEC; (b) RWMC; (c) TAN; (d) TRA.

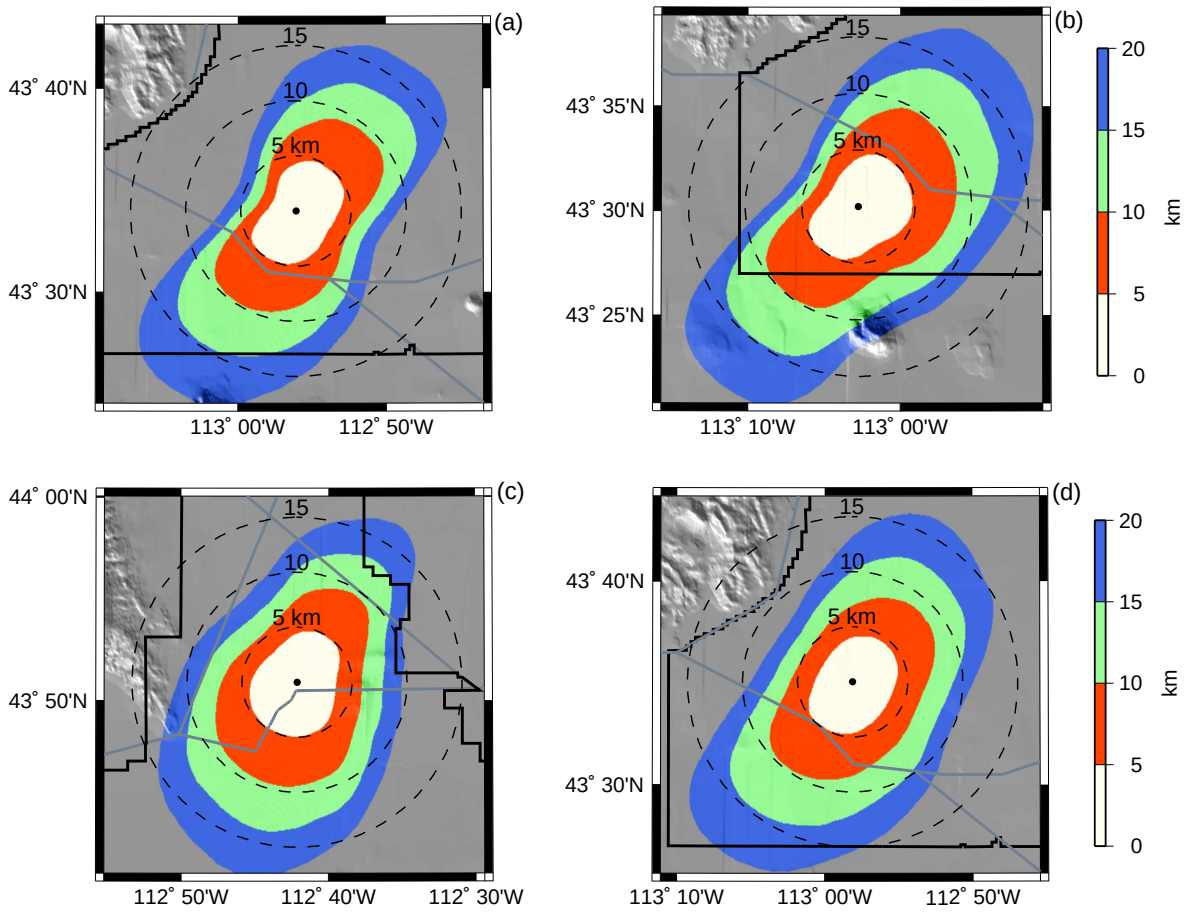

Figure 17: Contours of λ_a for surface releases from the four release locations. (a) INTEC; (b) RWMC; (c) TAN; (d) TRA.

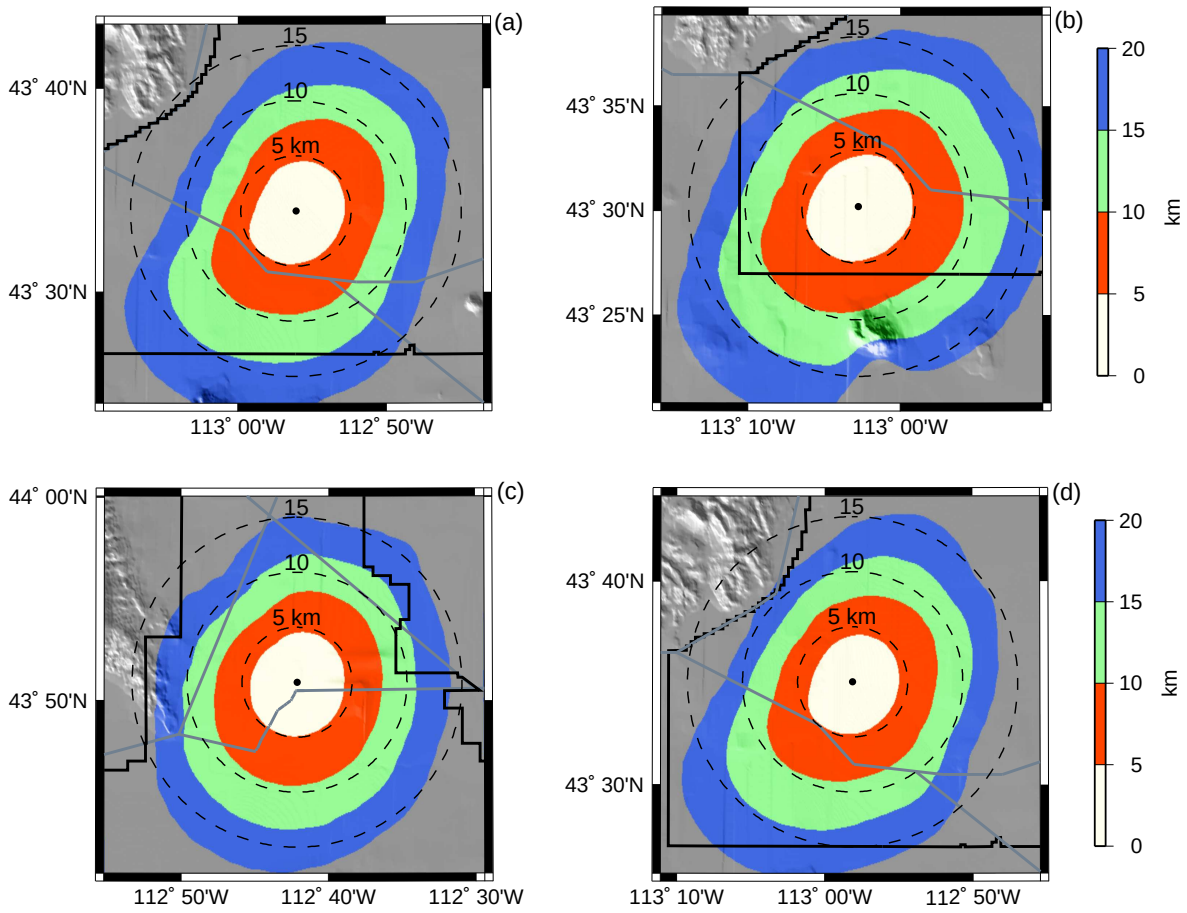

Figure 18: Contours of λ_c for surface releases from the four release locations. (a) INTEC; (b) RWMC; (c) TAN; (d) TRA.